



D3.1 – GUIDELINES FOR OPTIMISED SEMICONDUCTOR FABRICATION ROUTE

StretchBio – D3.1

Identifier:	StretchBio_D.3.1_Guidelines for optimized semiconductor fabrication route
Work package:	WP3
Dissemination level:	Public
Keywords:	Fabrication, nanopillars, cleanroom
Abstract:	This deliverable presents the results of the cleanroom fabrication work performed in the initial phase of the StretchBio project. Pillars with various pitch, diameter and heights have been fabricated. These results show that the required nanostructures can be fabricated with the desired dimensions and forms the basis of delivery of sample to consortium partners going forward in the project.



Document history:

Version	Date	Reason of change
1	09/02/2022	Creation of document
1.1	09/05/2022	1 st draft for consortium review
1.2	25/05/2022	Final draft
1.3	30/05/2022	Final version ready for submission

Document author(s):

Entity	Contributor
UB	Elena Lopez
DTU	Christian Bertelsen
UB	Francisco Hernandez Ramirez
UB	Albert Romano Rodríguez

Disclosure Statement:

This document has been produced by consortium partners of the *StretchBio* Horizon 2020 project, funded by the European Union's Horizon 2020 research and innovation programme under grant agreement No. 964808. The content of this document, the information contained herein, and the views expressed are those of the authors and do not necessarily reflect the official opinion of the European Union. Neither the European Union institutions and bodies nor any person acting on their behalf may be held responsible for the use which may be made of the information contained.



Executive Summary

This report is the first deliverable for WP3. It presents the fabrication route for the successful fabrication of the nanopillar arrays of different diameters, heights, and pitches.

It presents the fabrication approach for manufacturing nanopillars with radii of 45-120 nm and pitches of 300-500 nm. Specifically, we demonstrate nanopillars with radii of 100 nm and 120 nm, and pitches of 300 nm, 400 nm, and 500 nm. The fabrication process has been thoroughly tested, but changes in the conditions of the fabrication equipment means that the process must be continuously fine-tuned in order to produce high quality nanostructures. We show that we can fabricate pillars with a target radius of 100 and 120 nm with a precision of 6 nm or better, and a standard deviation between the radii of pillars on the same chip of 3.1 nm or lower.

Finally, some possible alterations to the fabrication are discussed. Altering the etching gasses to improve biocompatibility, changing the pillar composition to improve mechanical performance, and developing the process to include hybrid lithography in anticipation of higher production volumes in the last phases of the project.

The fabrication process described in this report provides a solid foundation for production of nanostructures for the coming phases of the StretchBio project, while also keeping options open for future improvements and developments.



Table of Contents

EXECUTIVE SUMMARY	3
1 INTRODUCTION	7
1.1 PURPOSE OF THE DOCUMENT	7
1.2 SCOPE OF THE DOCUMENT	7
1.3 RELATED DOCUMENTS	7
2 FABRICATION OF SILICON NANOPILLARS	9
2.1 FACILITIES.....	9
2.2 GENERALIZED DESIGN.....	9
2.3 PROCESS REQUIREMENTS.....	11
2.4 PROCESS STEPS.....	12
2.5 PROCESS DESCRIPTION	12
2.6 PROCESS OPTIMIZATION.....	13
2.1 RESULTS AND EVALUATION.....	14
3 FURTHER FABRICATION OPTIONS	20
3.1 BIOCOMPATIBILITY ISSUES.....	20
3.2 MECHANICAL PROPERTIES OF THE NANOPILLARS	20
3.3 CHALLENGES RELATED TO HIGH VOLUME-PRODUCTION.....	21
4 CONCLUSION	22
GLOSSARY.....	23
A. ANNEX – BIOCOMPATIBILITY ISSUES	24



List of Figures

Figure 1 – Facilities at DTU Nanolab. (Left) Cleanroom user operating the Jeol JBX-9500-FS electron beam writer inside the Nanolab cleanroom. (Right) Several cleanroom users in protective suits inside the Nanolab cleanroom. Images courtesy of DTU Nanolab.	9
Figure 2 – Sketch of the generalized design of the nanosensor shown from the top and from the side with a silicon structure (grey) on top of a silicon oxide substrate (blue). The sensor can be divided into three regions: coupling, waveguide, and photonic crystal regions as indicated in the sketch.	10
Figure 3 - Scanning electron microscope (SEM) image of the pillars tilted 30°. Nanograin structures can be observed standing between the pillars.	14
Figure 4 – 30° tilted SEM image of the nanopillars after optimization	14
Figure 5 - SEM top view images of the samples containing pillars with (Left) 100nm radii and 300 nm pitch, and (Right) 120 nm radii and 500 nm pitch	15
Figure 6 – Radii measurement distribution of the pillars shown in Figure 5. Dashed lines shown the theoretical radius of the fabricated pillars.	16
Figure 7 – (Left) SEM image of the deposited aluminum mask and the fitted circles. (Right) distribution of measured radii for the aluminum mask	17
Figure 8 – 90° side view SEM images of the pillars for samples with 100 nm radii and 300 nm pitch (left) and 120 nm radii and 500 nm pitch (right).....	18
Figure 9 – SEM image at 30° where the top of the pillars can be observed.....	18
Figure 10 - 20° tilted scanning electron microscope image showing the sidewalls of a CORE-etched wall (a) and trench (b).....	24



List of Tables

Table 1 – Overview of the key requirements for the fabrication of the photonic crystal.....	11
Table 2 – Overview of the process steps.....	12
Table 3 – Statistic figures for the radii measurement	16



1 Introduction

1.1 Purpose of the document

This report is the first deliverable for WP3. It presents the fabrication route for the successful fabrication of the nanopillar arrays of different diameters, heights, and pitches. For details on the overall project purpose, we refer to the project description given in the grant agreement.

1.2 Scope of the document

First and foremost, this report contains a detailed description of the current approach to the fabrication of the nanosensor that will be developed during the StretchBio project. The process can be used to fabricate nanopillars with radii of 45-120 nm and pitches of 300-500 nm. We also present the fabrication-related properties that are important to the performance of the sensor, such as sidewall angle and sidewall roughness, and evaluate the fabricated structures based on them. A brief description of the strengths and weaknesses of the fabrication approach is also provided.

Furthermore, a brief discussion of possible refinements of the process and future challenges is presented. While the current fabrication process produces high quality nanostructures, the requirements to the process will evolve once the complete sensor system is tested in the coming months. Currently, we anticipate four areas that may necessitate a refinement of the fabrications process:

- Biocompatibility issues
- Mechanical properties of the nanopillars
- Optical properties of the nanopillars
- Challenges related to high-volume production

To pre-emptively counter these challenges, we have begun looking into three process enhancements:

- Changing the etching process to obtain higher biocompatibility
- Investigating the use of composite pillars (both in geometry and materials), in agreement with results reported in D2.1
- Using a combination of lithography methods to increase the production output

Importantly, this report is not concerned with the details of the optical, mechanical, or biological functionality of the sensor, but strictly focuses on our ability to fabricate the desired nanostructures.

The deliverable concludes with a summary of the work completed at month 9 of the project and a description of the upcoming activities related to micro- and nanofabrication in the frame of WP3.

1.3 Related documents

This deliverable builds upon the findings made in D2.1 (Report on relation deformation-force for the nanopillars). It also supports and will be a starting point for the upcoming deliverables:



- D2.3 - Viability report on photonic sensors based on bending nanopillars
- D3.2 - Report on the bending-force relation in nanopillars
- D3.3 - Prototype of photonic nanosensor based on nanopillars
- D4.1 - Report on the nanopillar biocompatibility



2 Fabrication of silicon nanopillars

2.1 Facilities

The nanostructures are fabricated in the cleanroom facilities at the National Centre for Nanofabrication and Characterization (DTU Nanolab) located at the campus of the Technical University of Denmark (Kgs. Lyngby, Denmark). The facilities house a 1350 m² cleanroom with more than 150 high tech machines (see Figure 1 for examples) for fabrication and characterization of micro- and nanostructures. Access to the cleanroom is only available to trained scientists and each machine requires two training session with an experienced technician before the equipment can be freely used.



Figure 1 – Facilities at DTU Nanolab. (Left) Cleanroom user operating the Jeol JBX-9500-FS electron beam writer inside the Nanolab cleanroom. (Right) Several cleanroom users in protective suits inside the Nanolab cleanroom. Images courtesy of DTU Nanolab.

The air in the cleanroom is filtered many times a minute to remove airborne particles. This is necessary to produce the nanostructures needed in the StretchBio project, since even a single speck of dust would ruin the fabrication of the delicate nanostructures.

For further information about the facilities, visit DTU Nanolab’s website¹.

2.2 Generalized design

During the initial months of the project implementation, several variations of the detection concept have been proposed and tested by various project partners (see D2.1, and upcoming

¹ <https://www.nanolab.dtu.dk/english>



deliverables D2.3, D3.2, D4.1). As this is being written, the “final” device design is still under development.

Even so, Figure 2 shows a schematic with the key parts of the sensor that we expect will be part of the final device design (note that the drawing is not to scale, and that the actual design of each part may change parallel to the project development).

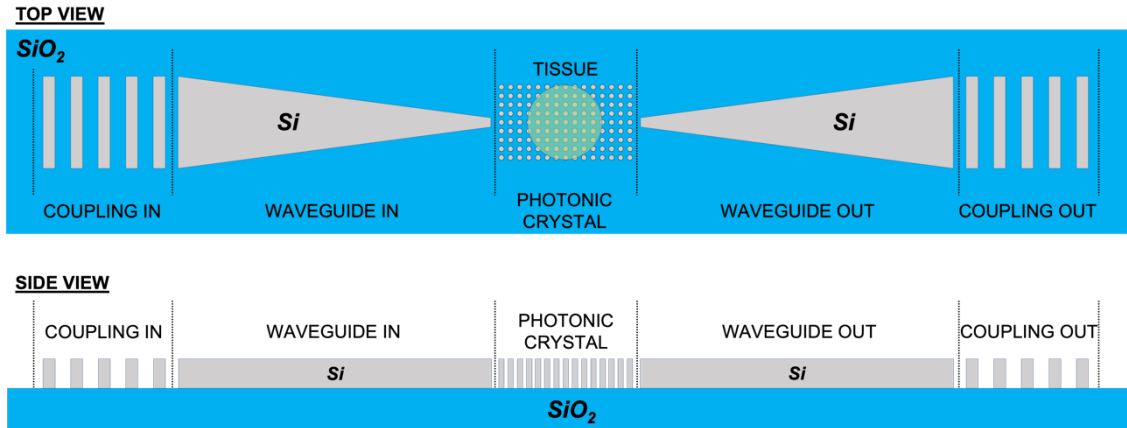


Figure 2 – Sketch of the generalized design of the nanosensor shown from the top and from the side with a silicon structure (grey) on top of a silicon oxide substrate (blue). The sensor can be divided into three regions: coupling, waveguide, and photonic crystal regions as indicated in the sketch.

The sensor can be divided into has three regions:

1. **Coupling regions**
A silicon grating for coupling the light into and out of the sensor. The final layout is still under discussion, but we expect grating dimensions from hundreds of nanometers to a few micrometer
2. **Tapered waveguide**
Guides the light from the grating structure ($\sim\mu\text{m}$) to the photonic crystal ($<100\text{ nm}$)
3. **Photonic crystal**
Nanopillar structure for detection of tissue forces with pillar diameters below $\sim 200\text{ nm}$

Due to the small size of the nanopillars in the photonic crystal region, it is the most challenging to fabricate and so far, most of our efforts have been focused on this region. It is however important that the fabrication process can accommodate the other regions equally well.

2.3 Process requirements

Before presenting the developed process, we will briefly outline the initial requirements for the fabrication of the photonic crystal.

Table 1 – Overview of the key requirements for the fabrication of the photonic crystal

Requirement	Description	Priority
Side wall angle	The angle between the bottom substrate and sidewall of the pillar should as close to 90° as possible. This is to ensure uniform optical performance from the top to the bottom of the photonic crystal.	High, especially for optical performance
Side wall roughness	The sidewall of the nanopillars should be as smooth as possible, with no bumps or scallops.	High, especially for optical performance
Side wall tapering	The side wall should be as straight as possible in order to have uniform mechanical and optical performance from the top to the bottom of the structure	High
Trench surface residues	The bottom substrate in between the nanopillars should be clear of any residue that affects the mechanical or optical performance of the sensor	High, for optical performance
Dimension precision	The dimensions of the nanostructure (diameter, pitch, and height) should be as close to the specified as possible	High
Top surface residues	The top surface of the pillars should be clear of any residue that affects the growth and adhesion of the tissue samples	Medium, potentially high for biocompatibility
Process flexibility	Process flexibility is desirable so that the dimensions of the sensor can be changed without reworking the process flow	Medium
Dimension variation	The variation in dimensions (pillar diameter, pillar height, etc.) should be as close to the specified across the entire structure, to ensure uniform optical and mechanical performance	Medium
Process time	Process time should be as short as possible to accommodate higher production volume later in the project	Low

The priorities of the requirements will be revisited over the course of the project if deemed necessary.



2.4 Process steps

The procedure described here is based on known and used techniques for micro- and nanofabrication. Even so, because of the high requirements of the proposed structures, fine tuning of the step conditions is essential. Thanks to this thorough optimization of parameters the fabrication of pillars with diameters down to 90 nm and heights of up to 3 μm has been possible. The process flow is described in Table 2 and detailed in the next subsection.

Table 2 – Overview of the process steps

Step	Process
1	Resist deposit
2	Discharge layer deposit
3	E-beam exposure
4	Development
5	Metallization
6	Lift-off
7	Dry etch

This process flow, which has been established on silicon substrates, has been further used for performing the test fabrication of nanopillars on Silicon on Insulator (SOI) substrates within the scope of this project. Small variations have been done depending on the purpose of the processed samples (e.g., biological tests, mechanical tests, optical tests, etc.). In addition, post processing such as laser cutting the samples is not considered in the above process flow and further steps might be needed in the future as stated in section 1.2.

2.5 Process description

For the fabrication of photonic crystals, 6" SOI substrates have been used. Provided by Siegert Wafer² (Aachen, Germany) the substrates have a top silicon (device) layer of 1.5 μm nominal thickness and a buried oxide (BOX) of 1 μm nominal thickness.

To obtain nanostructures with features below 100 nm the process requires the use of electron beam lithography. For this reason, the first 4 steps enumerated in Table 2 are related to the use of this technique. Firstly, the resist is deposited: due to the availability of resists in the nanofabrication center, AR-P 6200 (CSAR) resist is used in the described process. A spin-coated layer of 180 nm CSAR resist is deposited using a Süss MicroTec Gamma 4M Spin coater at 4000 rpm. Prior to the electron beam exposure, the deposition of a discharge layer is needed. Due to the insulator nature of the BOX layer of the SOI substrates, the discharge layer is needed to ensure electron evacuation during the exposure. If the layer is not deposited, electrons would remain in the device and resist layers spoiling the result of the lithography. A discharge layer of 20 nm Al is deposited using a Nano36 Thermal Evaporator System. After that, the sample is exposed inside a Jeol JBX-9500-FS electron beam writer, which operates at 100 keV. Depending on the minimum feature size on the prepared samples different conditions have been used, but typically currents below 20 nA are applied. After the exposure, the discharge layer is removed in a Laurel EDC 650 puddle developer, which sprays Tetramethylammonium Hydroxide (TMAH),

² <https://www.siegertwafer.com/>



during 60 s and, after that, in another Laurel EDC 650 puddle developer, the exposed resist is developed using AR-60-546 remover during 60 s.

Following the lithography, a metallization is needed to obtain the mask for the dry etch. To do so, 20 nm of electron beam evaporated Al is deposited at a rate of 2 Å/s and using a Temescal e-beam evaporator. After this, a lift-off process is carried out submerging the sample in a Remover 1165 bath with simultaneous ultrasonic agitation. This step allows the remaining resist with the layer of Al on top to be removed, leaving only the Al directly deposited in contact with the substrate. After the bath, the sample is cleaned in 2-propanol and rinsed in water and spin-dried.

Finally, the nanostructures are etched using reactive ion etching technique. The main reason to use a dry etch process is the anisotropy of the etch performance of this technique. Due to the need of having very vertical sidewalls of the structures for this project, a wet etching process is not suited. The reactive ion etching process used allows the simultaneous etching of the horizontal opened surfaces (without Al masking) and the passivation of the vertical sidewalls to prevent horizontal etching. To do so, C₄F₈ and SF₆ gases are used for passivating and etch, respectively, and with concentrations of 71 and 42 sccm. In addition, the Powers of the coil and the platen are controlled as well to increase the directionality of the process. Respectively, they are set to 1200 and 20 Watt. Finally, the temperature of the process has been set to -19°C. This last step is crucial for the success of the nanofabrication process and further investigation and optimization must be performed to perfect it.

2.6 Process optimization

Even though the process described above uses techniques that have been known and used for decades, exhaustive optimization has been needed to successfully fabricate the desired structures. The key step for the success of the fabrication of the pillars has been the reactive ion etching step. However, due to the natural degradation of the machines in the clean room facilities due to their use variations of these optimal conditions cannot be avoided. For this reason, periodic quality controls will be conducted to ensure the quality of the fabricated structures and, if needed, the readjustment of parameters will be considered.

The so-called pseudo-Bosch process is used for the silicon etch. The Bosch process is known to be a cyclic process where protection of the walls (passivation) and bombardment of the horizontal non masked areas (etch) steps are alternated. This process is one of the most used for silicon etching. However, due to this alternation of steps the side walls obtained using a Bosch process have a serration profile. For this reason, we avoided this effect using the pseudo-Bosch process where the passivation and etching are simultaneous.

Further optimization has been carried out because of the presence of non-desired nanostructured nanofilaments between the pillars that can be observed (Figure 3). Nanograss is a common by-product of the Bosch and pseudo-Bosch processes. Its presence between the pillars might affect the photonic properties of the system.



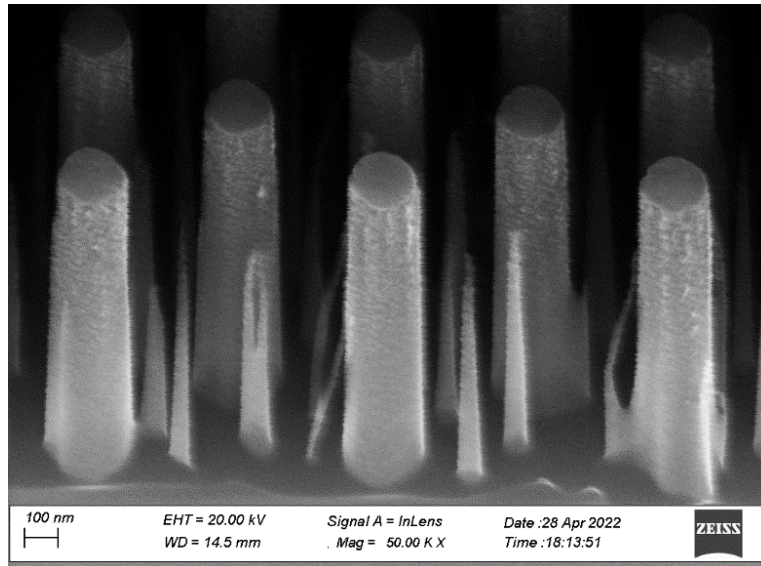


Figure 3 - Scanning electron microscope (SEM) image of the pillars tilted 30°. Nanograss structures can be observed standing between the pillars.

The presence of these nanostructures can be avoided by tuning the gas proportions. The sample shown in Figure 3 uses a ratio of 69/44 sccm of C_4F_8 and SF_6 gas, while in the sample shown in Figure 4 a ratio of 71/42 sccm was used instead. Comparing these two images, it is clear that a reduction of the nanograss presence and an improvement of the pillar shape occurs at the latter gas combination. Furthermore, it must be highlighted how a 2 sccm variation in the gas flows impacts the sensitivity of the process and the importance of the optimization steps and the periodic quality control that needs to be done.

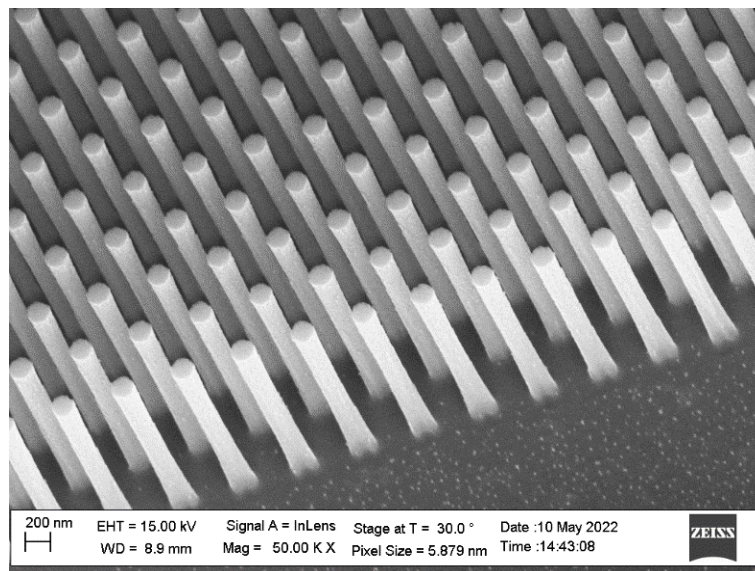


Figure 4 – 30° tilted SEM image of the nanopillars after optimization

2.1 Results and evaluation

The process described in the previous subsection has proven to be successful in the fabrication of the photonic structures required for StretchBio.



As listed in Table 1, there are some requirements that have been used to assess the quality of the obtained structures. Below, we evaluate the meeting of these requirements on the silicon substrates with photonic crystals based on pillars, with combinations of radii of 100 nm and 120 nm, and pitches of 300 nm, 400 nm, and 500 nm (see Figure 5).

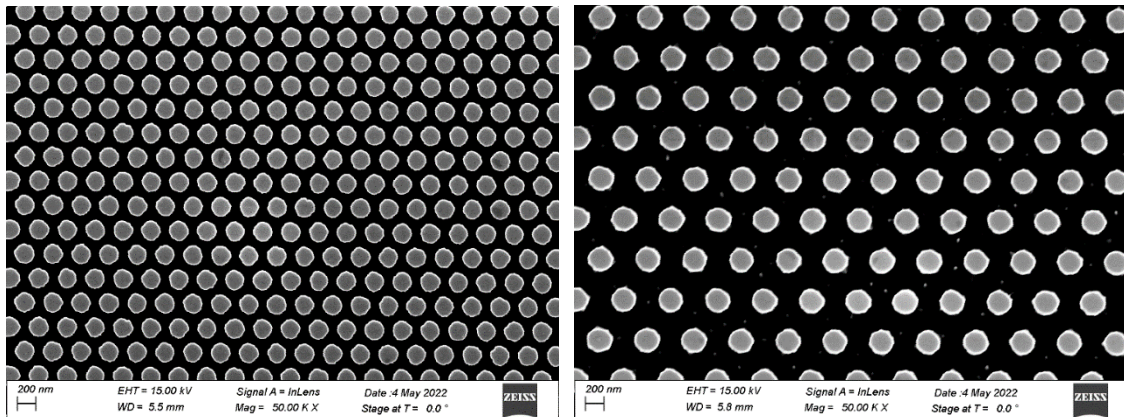


Figure 5 - SEM top view images of the samples containing pillars with (Left) 100nm radii and 300 nm pitch, and (Right) 120 nm radii and 500 nm pitch

Knowing the significant role that geometry plays in the properties of photonic crystals, ensuring that the pillars have the expected geometry and distribution is crucial. For this reason, a MATLAB-script (MATLAB R2021b) has been developed that allows the evaluation of the average pillar radius and distribution. The script uses the built-in MATLAB-function³ 'imfindcircles' which is part of the 'Image Processing Toolbox'⁴ to find the position and radii of circles in an image (i.e., like the SEM image shown in Figure 5). To conduct this analysis images from different regions of the same samples (i.e., that have undergone the same process) have been analyzed using the script. In Figure 6, the distribution of measured radii is shown for four samples (pitch of 300, 400 and 500 nm and radii of 100 and 120 nm). The mean value and the standard deviation of the radii of the three different samples are summarized in Table 3.

³ <https://se.mathworks.com/help/images/ref/imfindcircles.html>

⁴ <https://se.mathworks.com/products/image.html>



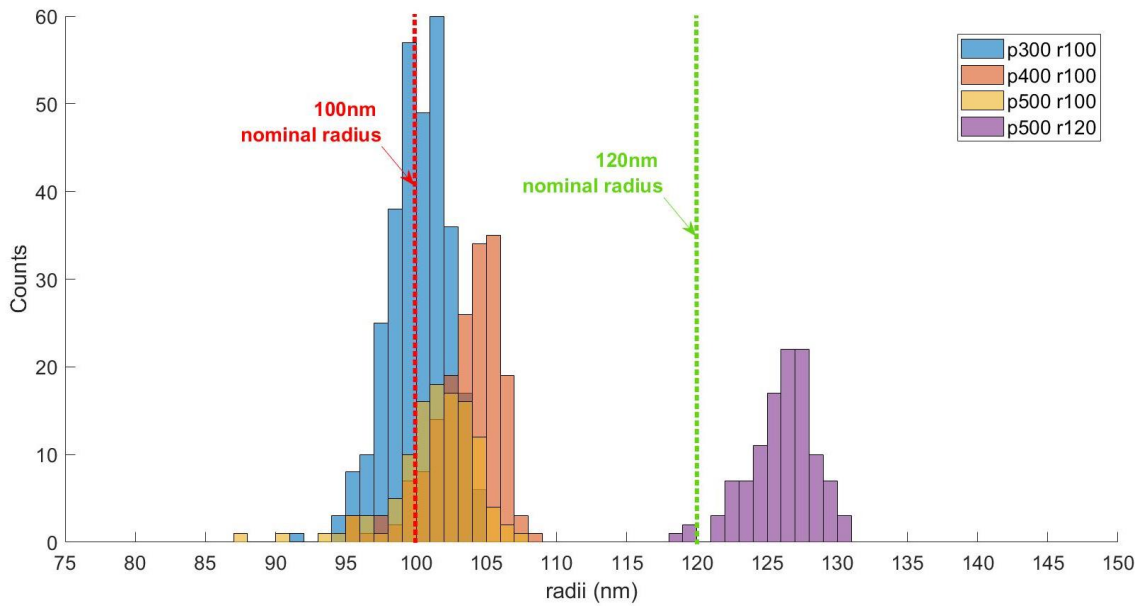


Figure 6 – Radii measurement distribution of the pillars shown in Figure 5. Dashed lines shown the theoretical radius of the fabricated pillars.

As can be seen, the average radius of the pillars is slightly larger than expected. This variability, however, is seen to be below 10 nm in all cases. The reason of this fluctuation might be due to proximity effects during the exposure or fluctuations in the reactive ion etching process.

Table 3 – Statistic figures for the radii measurement

Nominal		No. of pillars	Mean radius [nm]	Std. Dev. [nm]
Pitch [nm]	Radius [nm]			
300	100	310	100.2	2.1
400	100	175	103.6	2.5
500	100	112	101.4	3.1
500	120	112	126.1	2.3



Figure 7 show a SEM image of the aluminum mask used for etching and the measured radii of the mask for a sample with a target radius of 100 nm. It is seen that the mask radius corresponds well to the expected value.

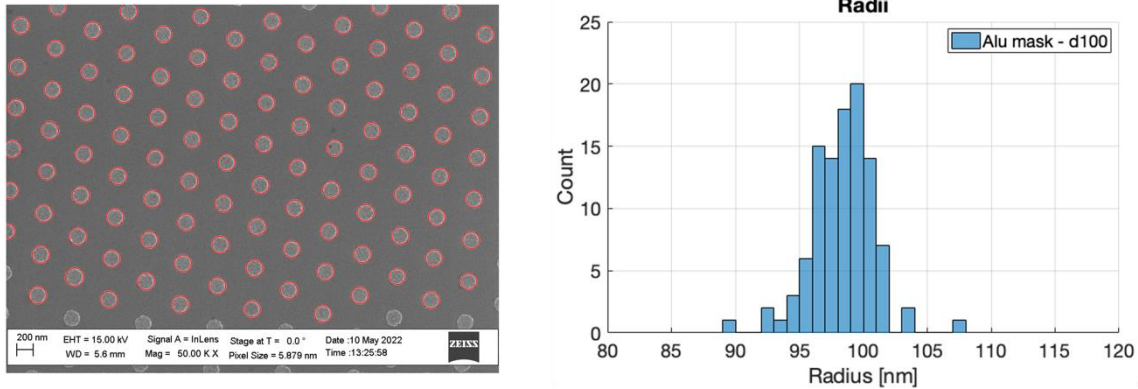


Figure 7 – (Left) SEM image of the deposited aluminum mask and the fitted circles. (Right) distribution of measured radii for the aluminum mask

In addition, due to the automatization of the calculus of these values variations among the SEM images can affect the accuracy of the measurement as well. But, as we already said, the variation from the nominal value is below 10 nm including the standard deviation therefore we can assume that the results are within the expected values. Nevertheless, with the current results and volume of samples fabricated we cannot ensure what is the nature of this error and if it is consistent or varies with time. In the first case changes in the masking size can be done to better approach to the nominal value, but in the latest this is not an option. For this reason, a systematic quality control of the samples must be carried out to always ensure the best results for future batches.

Another factor that might impact on the structure's performance is the pillar's side walls properties. To evaluate them, we have considered the roughness of the walls, the side wall angle and the side wall tapering of the pillars. These properties are essentially governed by the dry etching steps.

In Figure 8, the side views of the pillars for the different samples are shown. Cylindrical shaped pillars are etched with heights of approximately 1.6 μm . This etched depth is strongly dependent on the etching step duration. At the same time, the duration of the process is driven by the separation between the pillars and the surface of open areas compared with the masked ones (etch load). The aspect ratio between the etched depth and the opened space between pillars is limiting due to the ion transport through the etched spaces. If the spacing is very narrow and deep the etch rate decreases significantly due to the difficulty of ions to reach the bottom. On the other hand, the smallest the etch load the fastest and deepest the process will be since the concentration of reactants will be higher per unit of etched surface.

Considering these two limiting factors in our samples the only one what can have a real impact on the etching is the separation between the pillars. We can make this assumption since the masked area is small compared to the silicon surface of a 4" wafer. Therefore, the only relevant factor impacting the final etch rate and pillars profile is the separation between the pillars. In Figure 8 it can be seen how the sample with less space between the pillars (300 nm pitch and



100 nm radii) the etch at the bottom is narrower because of the difficulty of the reactants to reach the bottom. Meanwhile, the sample with broader spacing between the pillars this effect is not observed.

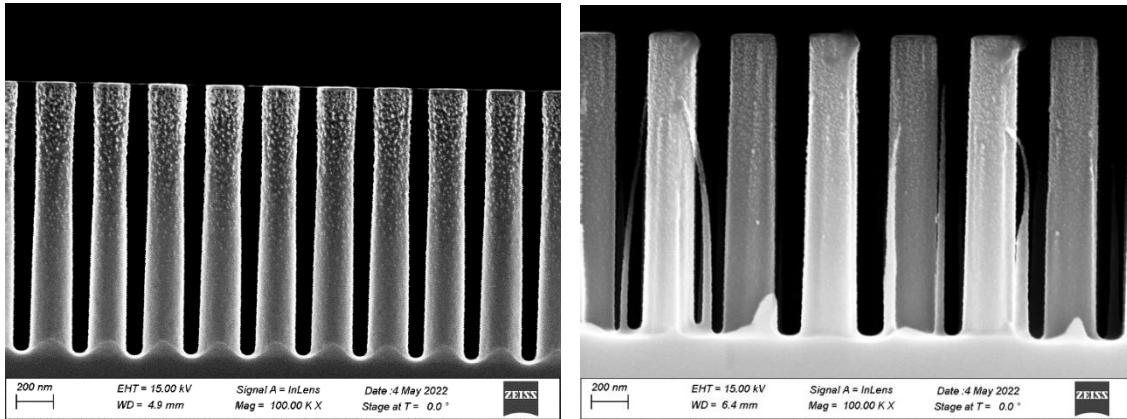


Figure 8 – 90° side view SEM images of the pillars for samples with 100 nm radii and 300 nm pitch (left) and 120 nm radii and 500 nm pitch (right)

Furthermore, it can be observed that the roughness of the side walls in all cases changes along the vertical direction, being more present on the top part of the pillars and decreasing towards the bottom. Insufficient passivation of the side walls could be one of the reasons why this roughness appears and specially at the pillar's top. However, as this is being written, further investigation must be done to study the appearance of this rough surface and to optimize the etch process to minimize this undesired effect. In Figure 9, a closer image of the roughness of the top of the pillars is shown: the remaining Al layer can still be observed on top of the silicon nanostructures and seems to be in good condition.

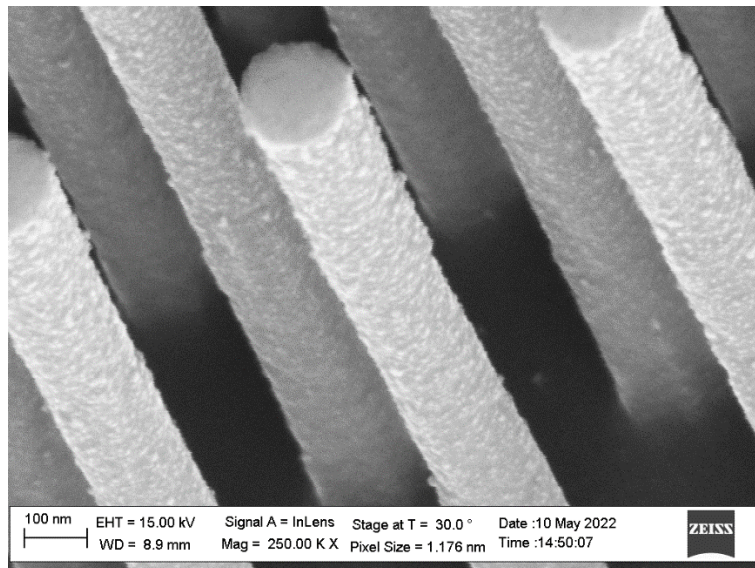


Figure 9 – SEM image at 30° where the top of the pillars can be observed

As can be seen, overall, the process results in the desired nanostructures that be used in further steps of the project. However, it must be further optimized and developed to avoid undesired artifacts that may jeopardize the sensors' performance. This pending refinement step is not

considered a major drawback since, thanks to the versatility and flexibility of the fabrication techniques, more controlled outputs will come in the mid-term.



3 Further fabrication options

The requirements to the fabrication process will evolve during the course of the project as the sensor system is tested and refined. Now, we foresee four main aspects that may require changes to the fabrications process:

- Biocompatibility issues
- Mechanical properties of the nanopillars
- Optical properties of the nanopillars
- Challenges related to high-volume production

In this section we will briefly describe some of the initial steps we have taken to preemptively counter this issue and improve the fabrication process.

3.1 Biocompatibility issues

A new etching process under evaluation is expected to enhance biocompatibility and remove undesired deposition of material during the etching. We believe that the results are potentially publishable. Further details are given in Annex A (labelled as confidential by the Consortium).

3.2 Mechanical properties of the nanopillars

In the frame of WP2 (deliverable D2.1), it was determined that taller pillars ($>2\ \mu\text{m}$) lead to larger deflection of the pillar tip when an equivalent force is applied, which significantly improves the sensitivity of the nanosensor. However, to contain the light inside the photonic crystal, the height of the light-guiding structure should be kept relatively low ($<1\ \mu\text{m}$ – see deliverable D2.2).

A solution to this challenge is the fabrication of composite pillars made of two different materials, e.g., silicon and silicon oxide (SiO_2). The idea is that the pillars can be tall enough to deflect significantly under load, but that the difference in refractive index between the two materials contains the light in the relatively shallower top part of the pillar. In this way, an array of composite pillars would perform optimally from both a mechanical and optical point of view (at least on paper).

However, fabrication of composite pillars is not easy due to the lack of etching agents used in RIE that are effective against SiO_2 , but not silicon. The problem is further complicated by the fact that the SiO_2 is positioned underneath the silicon making it very difficult to protect the silicon during the etching. Some processes have been developed that provides good selectivity (16:1) between silicon and SiO_2 ⁵, but they rely on a change in etching gasses that is not currently available at the cleanroom facilities at DTU.

Alternatively, a wet etching technique can be used to etch the SiO_2 . The most common approach is to use buffered hydrofluoric acid (BHF) in an isotropic etch, which will undercut the silicon structures. However, the process is difficult to control due to the relatively high etch rates (~ 80

⁵ M. Zhang and P. Watson, "Reactive Ion Etching Selectivity of Si/SiO₂: Comparing of two fluorocarbon gases CHF₃ and CF₄," p. 6, 2019.



nm/min) combined with the trouble of removing the etchant efficiently from the nanostructures.

In conclusion, while composite silicon/SiO₂ are promising due to their potential mechanical and optical performance, the very significant fabrication challenges involved in making them means that they should only be pursued if the regular pillars do not show the desired performance.

3.3 Challenges related to high volume-production

The standard process presented in this report considers the production of the chips in one run. This means that the exposure step is limited by the minimum feature size on the chip. Therefore, since the pillars creating the photonic crystal have diameters on the range of hundreds of nanometers the exposure must be done using electron beam lithography, which is slow, expensive, and unnecessary for features larger than a few micrometers.

For this reason, we will explore the combination of ultraviolet (UV) and electron beam lithography techniques. The preferred approach will be to first expose the parts of the sample with feature sizes is below one micrometer in the electron beam writer and perform the rest of the process until the lift-off step. Then, perform the UV lithography to transfer the above micrometer-sized features on the chips. To avoid stitching problems, alignment elements can be added to the exposed masks to ensure the correct assembly of the different elements during the exposures. After the UV exposure the process flow already described could be carried out until the end.

Even though this approach adds some extra steps to the process described in Table 2 we are convinced it will make the end-to-end process more efficient and versatile. Firstly, because of the scarce availability of the electron beam technique and its time-consuming overall operation (not only exposure time). In addition, with UV lithography the full wafer surface can be exposed at once if a physical mask is used, then once a final design is set the exposure of the above one-micron features can be done faster.



4 Conclusion

In this report we have described the route for the successful fabrication of photonic crystals based on silicon nanopillars. Thanks to the process described, pillars with radii down to 45 nm and lengths up to 3 μm can be fabricated. It has been shown that despite the known techniques and processes used, a thorough process of optimization of the parameters has been needed.

Identifying the key requirements for optimal performance of the final device has allowed us to target those nanofabrication aspects to optimize. The results show how most of these requirements have been resolved thanks to the optimization previously mentioned. The process flow is based on an initial electron beam lithographic process, followed by a metallization and lift-off and ending with a dry etch of the pillars. It is the last step that has been most challenging to optimize. We have seen that the side wall and the tapering angle are vertical for a majority of the samples, but that etching parameters also affects this. The roughness of the side walls has been improved but further optimization must be carried out in order to remove unwanted residue that may hamper optical performance later on. It is already clear, that the presence of residues can be significantly reduced with to small variations of the gas flows during the etch.

We have also developed a method for the systematic evaluation of the pillar diameter to ensure the best sample production for the project requirements. Statistical analysis of the mean radius of the fabricated pillars shows a deviation of less than 6 nm from the nominal pillar dimensions proving the extreme accuracy of the fabrication process.

In addition, even though the final design of the device is not finalized yet, we have predicted future scenarios where the nanofabrication might be challenged again. We believe that this “thinking ahead” philosophy will allow us to be prepared for upcoming demands within the project. Among these future possibilities there are critical concerns such as the biocompatibility of the samples currently processed and the light confinement within the photonic crystal layer. For this reason, some of the possible complementary approaches have been enumerated and briefly discussed in this report proving the versatility of the fabrication process.



Glossary

Abbreviation	Explanation
BOX	Buried Oxide
C ₄ F ₈	Octafluorocyclobutane
CSAR	AR-P 6200
Sccm	Standard cubic centimeter per minute
SEM	Scanning Electron Microscope
SF ₆	Sulfur hexafluoride
Si	Silicon
SiO ₂	Silicon Oxide
SOI	Silicon on Insulator
TMAH	Tetramethylammonium Hydroxide
UV	Ultraviolet
WP	Work Package

